Key Points:
- Average cloud adiabaticity (α) over the Northeast Pacific Ocean was found to be 0.766 ± 0.134 based on airborne analysis of 86 cloud events
- Cloud droplet number concentration, droplet effective radius, relative dispersion, and rain rate are correlated with α
- Inclusion of α in calculations from satellite remote-sensing retrievals results in greater agreement with in situ values

Cloud Adiabaticity and Its Relationship to Marine Stratocumulus Characteristics Over the Northeast Pacific Ocean

Rachel A. Braun[1] (iD), Hossein Dadashazar[1] (iD), Alexander B. MacDonald[1] (iD), Ewan Crosbie[2,3] (iD), Haflidi H. Jonsson[4], Roy K. Woods[4] (iD), Richard C. Flagan[5] (iD), John H. Seinfeld[5] (iD), and Armin Sorooshian[1,6] (iD)

[1]Department of Chemical and Environmental Engineering, University of Arizona, Tucson, AZ, USA, [2]Science Systems and Applications, Inc., Hampton, VA, USA, [3]NASA Langley Research Center, Hampton, VA, USA, [4]Department of Meteorology, Naval Postgraduate School, Monterey, CA, USA, [5]Department of Chemical Engineering, California Institute of Technology, Pasadena, CA, USA, [6]Department of Hydrology and Atmospheric Sciences, University of Arizona, Tucson, AZ, USA

Abstract Cloud adiabaticity (α) is defined as the ratio of the actual liquid water path ($LWP_{measured}$) in a cloud to its corresponding adiabatic value (LWP_{ad}). Processes such as drizzle and entrainment can lead to subadiabatic $LWP_{measured}$. This study examines α and its relationship to microphysical properties for 86 cloud events over the Northeast Pacific Ocean based on data collected during four separate summertime airborne campaigns. For the study region, α was found to be 0.766 ± 0.134. For most cases, clouds with a low value of α were found to have lower droplet number concentration (N_d), higher droplet effective radius (r_e), higher relative dispersion (d), and higher rain rate (R). The subcloud aerosol concentration (N_a) was often less for the low-α cases. The relationship between α and the vertical profiles and cloud-top characteristics for both the cloud droplet-only spectrum and full spectrum (cloud and rain droplets) is also examined. Inclusion of rain droplets produced a larger change in d for the low-α clouds as compared to the high-α clouds. On average, R increased at cloud top for high-α clouds but decreased at cloud top for low-α clouds. Accounting for α when estimating N_d from Moderate Resolution Imaging Spectroradiometer retrievals results in better agreement with in situ N_d values. Results of this work motivate the need for additional focus on the factors governing α, such as cloud type, and implications of its value, especially for remote-sensing retrievals.

1. Introduction

Remote-sensing retrievals of cloud properties are useful as an alternative to in situ airborne measurements that are generally prohibitive in spatiotemporal coverage. However, assumptions relating to the adiabatic structure of clouds are necessary in order to characterize cloud parameters from remote-sensing retrievals (Bennartz, 2007; Kubar et al., 2009; Wood, 2012). Numerous parameters, often describing the same quantity but with different names, have been used to quantify the subadiabatic structure of clouds, including the subadiabatic fraction (F_r: Janssen et al., 2011), mixing parameter (β: Lim et al., 2016), adiabatic factor (f_{ad}: Merk et al., 2016), and adiabaticity (α: Kim et al., 2008; Min et al., 2012). These parameters typically describe the extent to which the measured liquid water path ($LWP_{measured}$, g/m²) deviates from the thermodynamically predicted adiabatic LWP (LWP_{ad}) in a cloud. Other parameters characterizing subadiabatic structure, such as the adiabatic cloud depth ratio (Chin et al., 2000), consider the difference in measured cloud depth from its adiabatic value. Parameterizations for f_{ad} based on cloud depth have also been used, based on observations of clouds thicker than 1 km (Wood et al., 2009). For the present study, subadiabatic structure is characterized using the parameter α, which is defined as the ratio of $LWP_{measured}$ to LWP_{ad}.

The adiabatic lapse rate (Γ_{ad}) describes the predicted change in liquid water content (LWC) with height in a cloud and is a function of temperature and pressure. There has been considerable variability in values used for Γ_{ad} and f_{ad} in studies of different regions around the planet (Table 1 of Merk et al., 2016), with some studies choosing constant values for these parameters and others calculating the values based on cloud properties. Assumptions made about the values of these parameters can affect the accuracy of remote-sensing retrievals. Janssen et al. (2011) found that the factors contributing to the highest uncertainty in remotely retrieved cloud droplet number concentration (N_d) and cloud depth (H) were Γ_{ad} and F_r. Min et al. (2012)
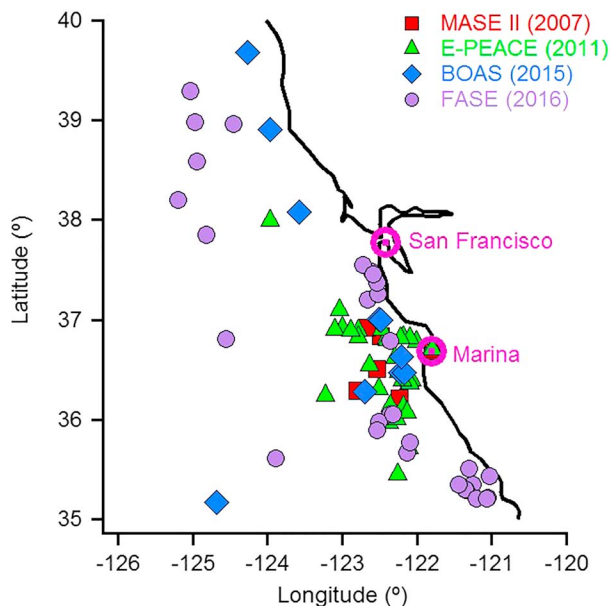
Figure 1. Region of the Northeastern Pacific Ocean adjacent to the California coast with the average location for each cloud sampling event. Marker color and shape correspond to the four different summertime campaigns. MASE II = Marine Stratus/Stratocumulus Experiment II; E-PEACE = Eastern Pacific Emitted Aerosol Cloud Experiment; BOAS = Biological and Oceanic Atmospheric Study; FASE = Fog and Stratocumulus Evolution Experiment.

showed that the inclusion of α, found using airborne data, in calculations of N_d using remote-sensing retrievals from the Moderate Resolution Imaging Spectroradiometer (MODIS) resulted in greater agreement with in situ values.

One possible explanation for the effect of adiabatic structure on remote-sensing cloud retrievals is the potential change in cloud response to aerosol loading as a function of cloud α. Previous studies have examined the impact of α on the aerosol first indirect effect, in which an increase in cloud condensation nuclei concentration (for a cloud at fixed LWP) results in smaller cloud droplets, a greater cloud N_d, and a larger cloud albedo (Twomey, 1977). Kim et al. (2008) found that while the aerosol first indirect effect was observed in the adiabatic regime, defined as $0.8 < α < 1.2$, clear evidence of this effect was absent in clouds with $0.1 < α < 0.8$. In contrast, McComiskey et al. (2009) found no dependence of the aerosol-cloud interaction (ACI) metric relating changes in cloud optical depth to aerosol perturbations (at fixed LWP) on α. While both studies examined nonprecipitating stratus clouds, the observed differences may be due to variations in the environmental conditions, namely, continental (Kim et al., 2008) versus coastal/marine (McComiskey et al., 2009) conditions. In addition, the subadiabatic structure of clouds is often due to cloud-top entrainment and can therefore impact the area in which remote-sensing retrievals obtain data (i.e., at cloud top).

One major region of cloud property interest is the Northeast (NE) Pacific Ocean due to the presence of a fairly consistent stratocumulus cloud deck (Wood, 2012). Marine stratocumulus have also been identified as a worthy subject of study in order to further understand the effects of feedback processes and buffering on the aerosol-cloud-precipitation system (Stevens & Feingold, 2009). Brenguier et al. (2003) commented on the ability of clouds in the NE Pacific Ocean region to achieve adiabatic structure using data from eight in situ cases. An assumption of adiabatic structure has been invoked in subsequent remote-sensing studies in the region (McComiskey et al., 2009). In the current study, 86 cloud events, spanning summertime campaigns from four different years over the NE Pacific Ocean, are examined using in situ airborne data. The present study seeks to quantify and examine (i) the adiabatic structure of clouds in the NE Pacific Ocean region, (ii) the relationships between microphysical cloud properties and α, (iii) the vertical profiles of microphysical cloud properties in relation to α, and (iv) the impact of α on remote-sensing retrievals in the study region.

2. Methodology

2.1. Airborne Data Collection

Data were collected over four airborne campaigns based in Marina, California, conducted with the Center for Interdisciplinary Remotely-Piloted Aircraft Studies (CIRPAS) Twin Otter. Figure 1 shows locations for 86 "cloud events" analyzed from flights during the Marine Stratus/Stratocumulus Experiment II (MASE II: 2007), the Eastern Pacific Emitted Aerosol Cloud Experiment (E-PEACE: 2011), the Biological and Oceanic Atmospheric Study (BOAS: 2015), and the Fog and Stratocumulus Evolution Experiment (FASE: 2016). A cloud event consists of an upward or downward pass through a cloud; a more detailed description of the determination of cloud events is given in section 2.2.

In each of the airborne campaigns, a suite of instruments was used to measure meteorological, aerosol, and cloud properties. LWC was measured using a PVM-100A probe (Gerber et al., 1994). Numerous cloud microphysical properties were calculated, including effective radius (r_e, μm), cloud droplet number concentration (N_d, cm^{-3}), and relative dispersion (d, ratio of standard deviation to mean radius of the droplet spectrum), using measurements from the Forward Scattering Spectrometer Probe (FSSP; Particle Measuring Systems, Inc., modified by Droplet Measurement Technologies [DMT], Inc.; d_p ~2 to ~46 μm) for MASE II, BOAS, and FASE and from the Cloud and Aerosol Spectrometer (CAS; DMT, Inc.; d_p ~0.6 to

~61 μm) forward scattering section for E-PEACE. Rain rates (R, mm/day) were calculated using drop distributions from the Cloud Imaging Probe (CIP; DMT, Inc.; d_p ~15 to ~1,560 μm) for MASE II, E-PEACE, and FASE, and equations for droplet terminal velocity (Zhang et al., 2001) and rain rate (Zhao et al., 2011). Due to lack of rain drop distribution measurements during BOAS, subsequent descriptions of R exclude cloud events from BOAS. Minimum cut-point diameters for cloud drops and rain drops were chosen as 4 and 40 μm, respectively, based on past work in the same study region (Chen et al., 2012). Subcloud aerosol (d_p ~0.1 to ~2.2 μm) concentrations were measured with a Passive Cavity Aerosol Spectrometer Probe (Particle Measuring Systems, Inc., modified by DMT, Inc.). Data from the aforementioned instruments were obtained at 1-Hz time resolution, and the aircraft typically flew at 55 m/s. Additional information about instrumentation for the various campaigns, including quality control details, can be found in Sorooshian et al. (2018).

2.2. Determination of Cloud Events

The presence of a cloud in this study is defined by the threshold value of LWC ≥ 0.02 g/m^3, following other studies in this region (Dadashazar et al., 2018; Prabhakar et al., 2014). The cloud events to be analyzed were chosen based on clear definition of cloud boundaries and minimization of in-cloud pockets of dry air. For each cloud event, no more than two in-cloud sample points of LWC dropped below the LWC threshold; furthermore, in the cases where two in-cloud samples dropped below the threshold, they were not adjacent points in time. Cloud boundaries were defined such that for 14 s upon leaving the cloud edge, the LWC did not exceed the LWC threshold. Due to differences in attack angle and flight patterns upon exiting the cloud, this 14-s time frame ranged from maximum heights of 5–68 m above the cloud and 14–92 m below the cloud. Table S1 found in the supporting information summarizes the spatiotemporal characteristics of the 86 cloud events analyzed in this study.

While the PVM-100A is widely used for in situ characterization of LWP (e.g., Min et al., 2012; Noh et al., 2013), it is limited in accuracy for measurement of droplets $>$~45 μm, above which the response gradually decreases to a ~50% underestimate in LWC at 70 μm (Gerber et al., 1994). Therefore, any LWC present in rain droplets is underestimated in the measurements, and LWP$_{measured}$ may be lower than the true value. While integration of the droplet spectrum from CAS or FSSP can also be used to calculate LWP, the maximum particle diameter measured by FSSP is only 46 μm, which is more limited than the size range measured by the PVM-100A. The CAS probe is able to measure larger sizes (maximum d_p = 61 μm) but is only available for E-PEACE. Therefore, to capture the widest possible spectrum of LWC and to maintain consistency in the calculation of LWP$_{measured}$ across all four campaigns, measurements from the PVM-100A were used to quantify LWP$_{measured}$.

Previous work has shown that MODIS retrievals are more strongly impacted by smaller as opposed to larger droplets (e.g., Boers et al., 1996; Stephens & Haynes, 2007) in light-drizzle conditions. For the 71 cloud events in the present study with data for R, 58 events had whole cloud mean R in the light-drizzle range ($R < 0.3$ mm/hr, as defined in the American Meteorological Society's Glossary). Therefore, in the present study it is likely that the greatest influence on MODIS retrievals for most of the cloud events examined is from the cloud droplet range (i.e., within the range of the PVM-100A).

2.3. Adiabaticity Calculations

Adiabaticity (α) is defined as the ratio of LWP$_{measured}$ to that of the thermodynamically predicted LWP$_{ad}$:

$$\alpha = \frac{\text{LWP}_{measured}}{\text{LWP}_{ad}} \tag{1}$$

While the theoretical maximum value of α is 1, previous studies have measured $\alpha > 1$, especially in clouds with $H < 450$ m (Miller et al., 1998). In the present study, two cloud events had $\alpha > 1$. Adiabatic LWP, calculated using equation (2), is a function of H and Γ_{ad}, which is determined by temperature and pressure at cloud base and assumed to be relatively constant throughout the cloud depth for shallow clouds, such as those in this study (Brenguier, 1991).
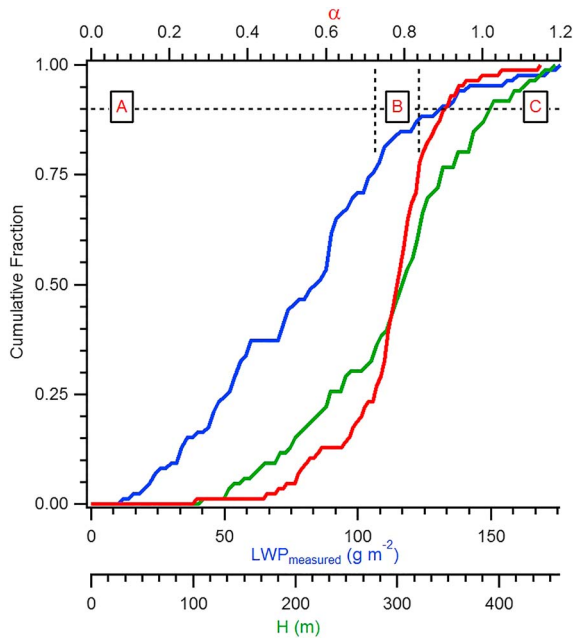
Figure 2. Cumulative fractions for the 86 cloud events showing adiabaticity (α), measured liquid water path ($LWP_{measured}$), and cloud depth (H). Categories A ($\alpha < 0.7255$), B ($0.7255 < \alpha < 0.8375$), and C ($\alpha > 0.8375$) are shown.

$$LWP_{ad} = \frac{1}{2} \Gamma_{ad} H^2 \qquad (2)$$

The methodology for calculating Γ_{ad} follows the description from Albrecht et al. (1990):

$$\Gamma_{ad} = \left[\frac{(\varepsilon + w_s)w_s l_v}{R_d T^2} \Gamma_w - \frac{g w_s P}{(P - e_s)R_d T} \right] \rho_d \qquad (3)$$

where R_d is the ideal gas constant for dry air, ε is the ratio of R_d to R_v (the ideal gas constant for water vapor), w_s is the saturation mixing ratio, l_v is the latent heat of vaporization, T is temperature, Γ_w is the moist adiabatic lapse rate (as defined in the American Meteorological Society's Glossary), g is the acceleration due to gravity, P is pressure, e_s is the saturation vapor pressure of water, and ρ_d is the density of dry air. Cloud base T was used to calculate e_s and l_v (Perry & Green, 2008), while both cloud base T and P were used in the calculation of w_s, Γ_w, ρ_d, and Γ_{ad}.

3. Results and Discussion

3.1. Northeastern Pacific Region Statistics

Remote-sensing studies use different values for adiabatic cloud parameters in different regions around the world (Merk et al., 2016). For the 86 cloud events analyzed over the NE Pacific Ocean in this study, the average ± standard deviation for Γ_{ad} and α were found to be 2.332 ± 0.075 g·m^{-3}·km^{-1} and 0.766 ± 0.134, respectively. These in situ results are similar to those previously reported in the study region, as determined by remote sensing, for Γ_{ad} (Albrecht et al., 1990) and α (0.71 ± 0.18 from Kim et al., 2012).

The distributions of α, $LWP_{measured}$, and H for the 86 cloud events are shown in Figure 2. These results for the NE Pacific are similar to those found in the Southeastern Pacific where the majority of cases were subadiabatic (Figure 3a of Min et al., 2012). For subsequent analysis, cloud events were divided into three α categories, as shown in Figure 2, based on the 25th and 75th percentiles of α for the 86 cloud events: category A (22 cloud events; $\alpha < 0.7255$), category B (42 cloud events; $0.7255 < \alpha < 0.8375$), and category C (22 cloud events; $\alpha > 0.8375$). Approximately half of the cases analyzed in this study had $\alpha \leq 0.8$, which is within the range described by Kim et al. (2008) in which no clear evidence of the aerosol first indirect effect was observed.

Previous studies have shown that α tends to decrease with increasing H (Merk et al., 2016; Min et al., 2012). Similar results were found in the present study for the NE Pacific region, as shown in Figure 3. This behavior is potentially due to the dependence of LWP_{ad} on H^2. For example, a 10% increase in H would correspond to a 21% increase in LWP in order to maintain a constant α. Therefore, it may be more difficult for deeper clouds to accumulate the necessary amount of LWC, in particular due to precipitation, in order to maintain a sufficiently high α.

In order to characterize the vertical profile of subadiabatic behavior in clouds, Figure 4 shows the change in $LWC_{measured}$ with change in height in cloud (z), normalized by the adiabatic value (Γ_{ad}), for each cloud thickness tenth. Values >1 correspond to LWC lapse rates greater than the adiabatic value, while values ≤ 1 indicate measured LWC lapse rates $\leq \Gamma_{ad}$. Negative values in the lower levels of the cloud describe locations where the $LWC_{measured}$ actually decreased with increasing height in cloud. Convection in the cloud layer could lead to in-cloud pockets of air that are either more moist or dry than expected, yielding decreases
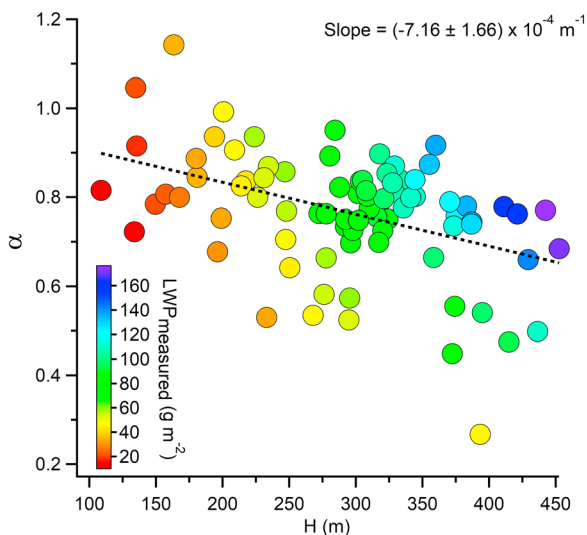

Figure 3. Adiabaticity (α) as a function of cloud depth (H), with color as a function of measured liquid water path ($LWP_{measured}$).
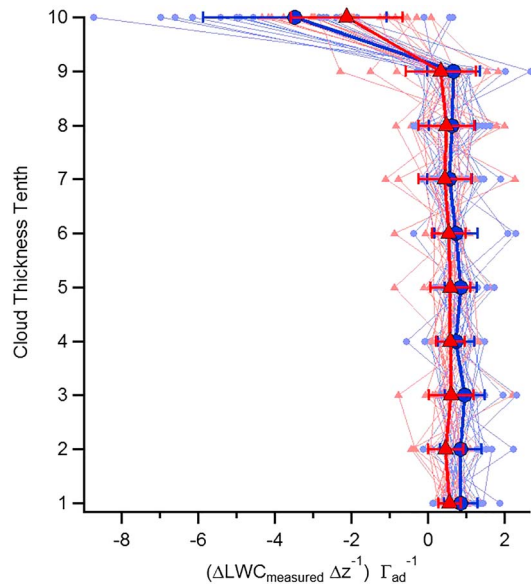
Figure 4. Ratio of change of $LWC_{measured}$ with height (z) to the adiabatic lapse rate (Γ_{ad}) for each cloud thickness tenth. Thin red (blue) lines are for individual cloud cases in α category A (C), while thick red (blue) lines represent the average for category A (C). Error bars represent ± 1 standard deviation from the mean value.

in $LWC_{measured}$ with increasing height. As summarized by Grosvenor et al. (2018), an assumption is typically made during characterizations of N_d from remote-sensing retrievals that LWC increases with increasing z at a constant fraction of its adiabatic value. The majority of cloud events in categories A and C exhibited fairly constant values in the bottom 90% of the cloud, with the events in category C having values closer to unity on average. This indicates that only in the bottom 90% of the cloud does the LWC lapse rate tend to remain a constant fraction of Γ_{ad}. However, in the top 10% of the cloud, a sharp decrease to negative values is observed for many of the cloud events. Previous studies have also shown that a deviation in LWC from its adiabatic value exists at cloud top (e.g., Albrecht et al., 1985; Painemal & Zuidema, 2011). One interesting note in Figure 4 is that, on average, the events in category C show larger decreases in LWC with z in the top 10% of the cloud than those events in category A. As will be discussed in section 3.3, more adiabatic clouds exhibited greater R at cloud top as compared to cloud base. Increased precipitation at cloud top could contribute to the noticeable decrease in LWC at cloud top. Furthermore, processes such as entrainment can lead to depletion of LWC in upper levels of the cloud. Therefore, for the cloud events observed, the measured LWC lapse rate does not appear to be a constant fraction of Γ_{ad} for the full depth of the cloud.

3.2. Relationship Between Cloud Microphysical Properties and Adiabaticity

3.2.1. Vertical Profiles for Low- and High-Adiabaticity Cloud Events

Because the deviation in LWC lapse rate from its adiabatic value is related to both in-cloud height and α, the vertical profiles of cloud microphysical properties are also likely to be impacted by α. Lim et al. (2016) demonstrated the correlation of the vertical structure of microphysical cloud properties (specifically N_d and r_e) with α. In order to determine the impacts of cloud α on microphysical properties, vertical profiles of N_d, r_e, d, and R are analyzed. Cloud events were binned by $LWP_{measured}$, in increments of 10 g/m^2 to reduce meteorological influences when examining differences in microphysical properties between low- and high-α cases (i.e. categories A and C, respectively). Because of the small variation in Γ_{ad} for the study region, clouds in category A are, by definition, thicker than those in category C for a given LWP. Figures S1–S11 in the supporting information show 3-s moving averages of microphysical characteristics for the cloud events in categories A and C; more detailed analyses for cloud events in two specific LWP bins is given in section 3.2.2. In general, less-adiabatic clouds exhibit lower N_d, higher r_e, higher d, and higher R throughout the whole cloud.

Subcloud aerosol concentrations (N_a) were also examined for each cloud event. Differences in N_a have been linked to changes in cloud microphysical properties such as N_d (Twomey, 1974), d (Lu & Seinfeld, 2006), and r_e/R (Sorooshian et al., 2010). Numerous parameterizations have been proposed to examine the impacts of aerosols on cloud microphysical properties (Feingold et al., 2001). For the current study, the following parameterization of ACI was chosen because it does not require constant macrophysical cloud properties (e.g., LWP):

$$ACI_N = \frac{d \ln N_d}{d \ln N_a} \qquad (4)$$

where N_d is the average cloud droplet number concentration in the cloud and N_a is the average subcloud aerosol concentration (McComiskey et al., 2009). The ACI analysis appears to show an increase in ACI_N as α decreases, based on the three α categories (supporting information Figure S12). While the ACI_N values for categories B ($ACI_N = 0.59$) and C ($ACI_N = 0.54$) are comparable to previous studies in the region (e.g., 0.48 from McComiskey et al., 2009), the value for category A is much greater ($ACI_N = 0.93$). Additional in situ measurements would be needed to determine if this result is representative of typical subadiabatic clouds in the NE Pacific or rather an artifact from a low number of sample points (22 events in category A in the present study versus 20,996 observations from McComiskey et al., 2009).

One interesting note is that the subcloud aerosol concentration (N_a) was often less for low-α events than high-α ones in the same LWP bin. The observed relationship between low α, reduced subcloud N_a, and increased R could be explained by several mechanisms. Lower subcloud N_a could result in an increase in R that would reduce $LWP_{measured}$ and therefore also reduce α. In addition, higher R from low-α clouds could increase wet scavenging of aerosols and lead to cleaner conditions below the cloud (MacDonald et al., 2018); this factor serves as a plausible explanation for why ACI_N was most enhanced for the low-α clouds, supported by past work pointing to a link between enhanced wet scavenging and higher ACI values (Duong et al., 2011).

Following the method of Brenguier et al. (2003), cloud events were also divided into fifths by height so as to further analyze the vertical structure of microphysical properties. Figure 5 shows vertical profiles of N_d and r_e normalized by the value for the cloud bottom thickness fifth, in the lowest- and highest-α categories (A and C, respectively) when considering the cloud droplet-only spectrum (d_p ~4 to ~40 μm) and the full droplet spectrum (cloud and rain droplets: d_p ~ 4 to ~1,560 μm). With increasing height, N_d tends to increase until the top thickness fifth of the cloud, at which point the trend reverses. This decrease in N_d at cloud top could potentially signify inhomogeneous mixing, whereby entrainment of dry air from above leads to dilution of the air parcel and therefore a lower N_d. A common description of cloud-top entrainment separates mixing behavior into categories of homogeneous mixing, inhomogeneous mixing, or some combination of the two (Baker et al., 1982). Previous studies have noted the complexity of addressing the question of whether inhomogeneous or homogeneous mixing occurs due to cloud-top entrainment owing to discrepancies between the spatiotemporal scales of entrainment processes and airborne measurements (Burnet & Brenguier, 2007; Yum et al., 2015). However, both inhomogeneous (e.g., Gerber et al., 2013; Lu et al., 2011) and homogenous (e.g., Yeom et al., 2017) mixing have been assigned as the dominant mixing entrainment process in stratocumulus clouds. Yeom et al. (2017) noted that because the continental stratocumulus they observed had much higher relative humidity (RH) above cloud top as compared to the study of marine stratocumulus by Yum et al. (2015), homogeneous mixing was favorable. In the present study, above-cloud RH was closer to that observed by Yeom et al. (2017), with an average RH value of approximately 70% in the first 30 m above cloud top for all cloud events studied. While additional analysis of the measured properties at and around the cloud top could potentially answer the question as to which mixing mechanism dominates the cloud-top entrainment observed, such analysis is beyond the scope of the present study. Other processes that could lead to a decrease in N_d include increased precipitation at cloud top, as will be shown in section 3.3 for the high-α cases. The vertical profile of N_d in both categories A and C remains relatively unchanged by the addition of the rain droplet spectrum. Category C shows greater values of N_d, as normalized by the cloud thickness bottom fifth, than category A (Figures 5a and 5b). With increasing height in cloud, r_e increases (as compared to the cloud thickness bottom fifth) for both categories A and C, with category A showing a larger increase in r_e with height (Figure 5c). However, upon inclusion of rain droplets, as shown in Figure 5d, both categories demonstrate a reduced increase in r_e with height in the cloud. In contrast to consideration of solely the cloud droplet spectrum, category A shows a more homogeneous vertical profile of r_e than category C for the full droplet spectrum. Martin et al. (1994) demonstrated that changes in spectral shape due to the consideration of drizzle-size droplets in addition to cloud droplets can impact the parameterization of r_e. The aforementioned differences in Figure 5c versus Figure 5d can potentially be explained by the shape of the droplet size distribution, which is discussed next in the context of the d parameter.

Previous studies have demonstrated relationships between d and autoconversion (Liu & Daum, 2004) and radiative forcing (Liu et al., 2008; Rotstayn & Liu, 2003, 2005). In order to study the vertical structure of d in the examined clouds, Figure 6a displays results for d of the cloud droplet-only spectrum in each cloud thickness fifth based on α category, while Figure 6b shows d for the full droplet spectrum. Both categories follow a trend of decreasing d with increasing height in cloud, similar to previous in situ measurements (Pawlowska et al., 2006). On average, the cloud events with higher α exhibit lower d than those in the low-α category. Figure 6c shows the percent change in d between the cloud droplet spectrum and the full droplet spectrum. The inclusion of rain droplets in the spectrum increases the d in each cloud thickness fifth by approximately 9.6–12.4% on average for the high-α cloud events. However, for the low-α cases, the percent increase in d is on average nearly double that of the percent change for the highly adiabatic clouds and decreases with increasing height in cloud from 26.6% for the bottom thickness fifth to approximately 17.8% in the top
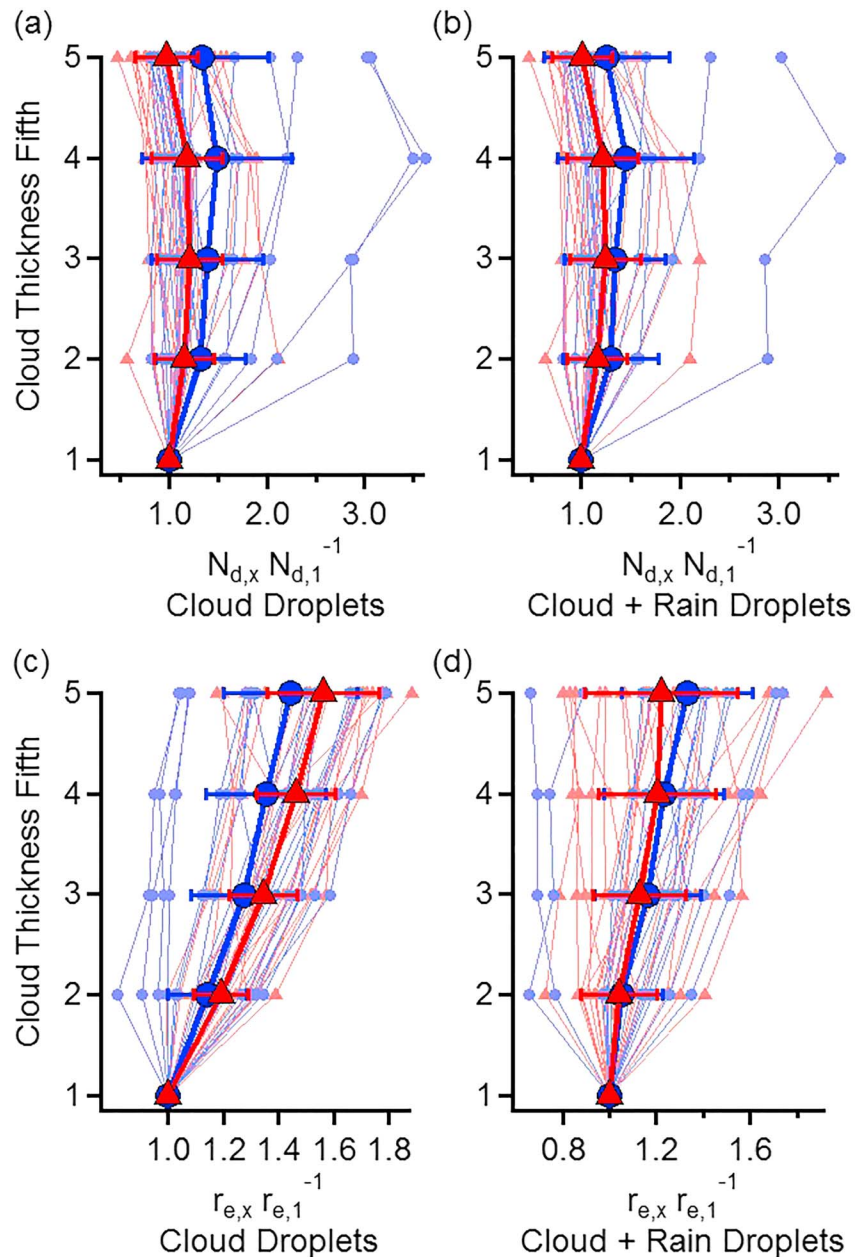
Figure 5. Vertical profiles of N_d and r_e for each cloud thickness fifth for (a, c) the cloud droplet-only spectrum (4 to 40 μm) and (b, d) the full (cloud and rain) droplet (4 to ~1,560 μm) spectrum. Values are normalized by the bottom thickness fifth of the cloud (i.e., $N_{d,x}/N_{d,1}$, where x is the number of the cloud thickness fifth and 1 is the bottom thickness fifth of the cloud). Thin red (blue) lines are for individual cloud cases in α category A (C), while thick red (blue) lines represent the average for category A (C). Error bars represent ±1 standard deviation from the mean value.

thickness fifth of the cloud. Using large eddy simulations, Lu and Seinfeld (2006) found that the inclusion of rain droplets in addition to cloud droplets for d calculations resulted in almost no change in d for a weakly drizzling case and a small increase in d for a more heavily drizzling case. The results of the present study appear to be in agreement with that finding since the low-α cases typically exhibited enhanced R compared to high-α cases in the same LWP bin.

For both Figures 5 and 6, average values of the cloud microphysical properties for α category B were typically between those of categories A and C. Figures S13 and S14 in the supporting information show averages and standard deviations for all three categories, analogous to Figures 5 and 6.
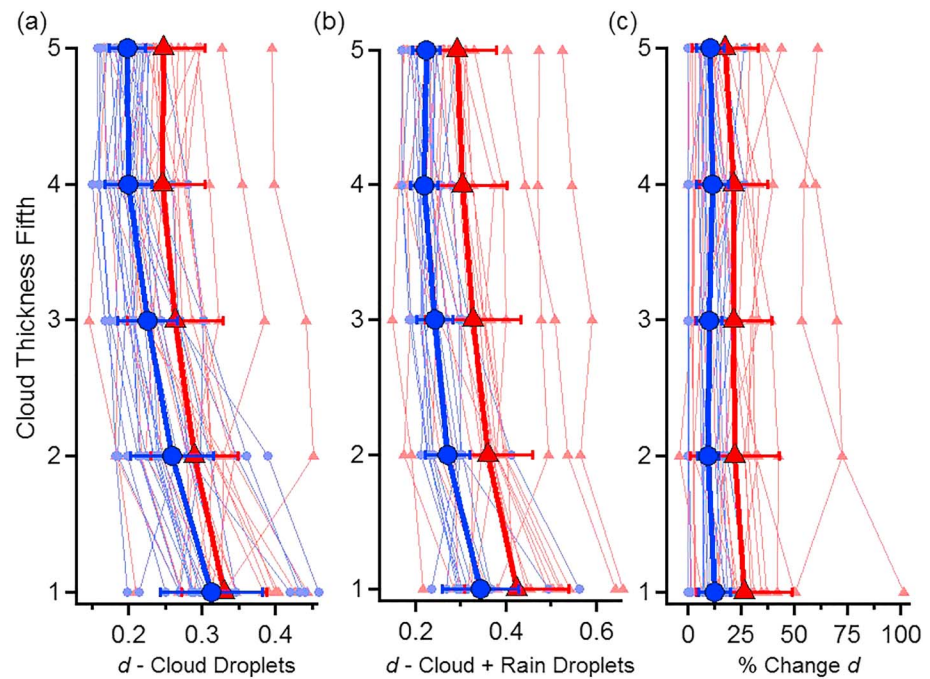
Figure 6. Vertical profiles of relative dispersion (d) averaged for each cloud thickness fifth for: A the cloud droplet-only spectrum (4 to 40 μm), b the full (cloud and rain) droplet (4 to ~1,560 μm) spectrum, and c the percent change in d upon considering the rain droplets in addition to the cloud droplets. Thin red (blue) lines are for individual cloud cases in α category A (C), while thick red (blue) lines represent the average for category A (C). Error bars represent $\pm$ one standard deviation from the mean value.

3.2.2. Case Studies

Two case studies were chosen in order to more closely examine differences in cloud microphysical properties between low- and high-α cloud events. The first case study chosen represents vertical profiles of microphysical properties that are fairly typical of the majority of the LWP$_{measured}$ bins, while the second case study shows different behavior for some, but not all, of the microphysical properties.

The first case study is for a single cloud event in category A (A1) and two events in category C (C1 and C2) that fall into the LWP$_{measured}$ bin of 104–114 g/m^2. As shown in Figure 7, the vertical profiles of microphysical properties of these cloud events are fairly representative of the behavior observed in the majority of cases. For cloud events in the same LWP bin, cloud events in category A typically display lower N_d, higher r_e, higher d, and higher R throughout the whole depth of the cloud. While R is comparable between the three cases for the cloud thickness top fifth (A1 = 6.28 mm/day versus C1 = 6.95 mm/day and C2 = 6.30 mm/day), its value is much higher on average for the bottom 80% of the low-α cloud event (12.53 mm/day for A1 versus 4.04 and 3.42 mm/day for C1 and C2, respectively). Furthermore, subcloud N_a is lower for the event in category A (133 cm^{-3}), as compared to the two events in category C (184 and 302 cm^{-3}). As previously postulated in section 3.2.1, this difference in N_a could be the result of a greater wet scavenging rate due to a higher R in the bottom portion of cloud A1.

Figure 8 shows the cloud and rain droplet size distributions for the three cloud events. Event A1 exhibited a fairly constant droplet size distribution profile, consistently extending to ~200 μm, with increasing height in cloud. For events C1 and C2, the rain droplet concentrations appear to be less uniform with altitude than those in A1; R for the two high-α events appears to be driven mainly by a few areas with very large rain droplets, particularly in the top part of the cloud.

The second case study is for the LWP$_{measured}$ range of 131.5–141.5 g/m^2, which contained one cloud event from category A (A1) and two cloud events from category C (C1 and C2; Figure 9). In contrast to most of the other LWP$_{measured}$ bins and the first case study, the cloud event in category A exhibited a higher N_d, lower r_e, and higher subcloud N_a than the cloud events in category C. However, the cloud columnar-mean values of
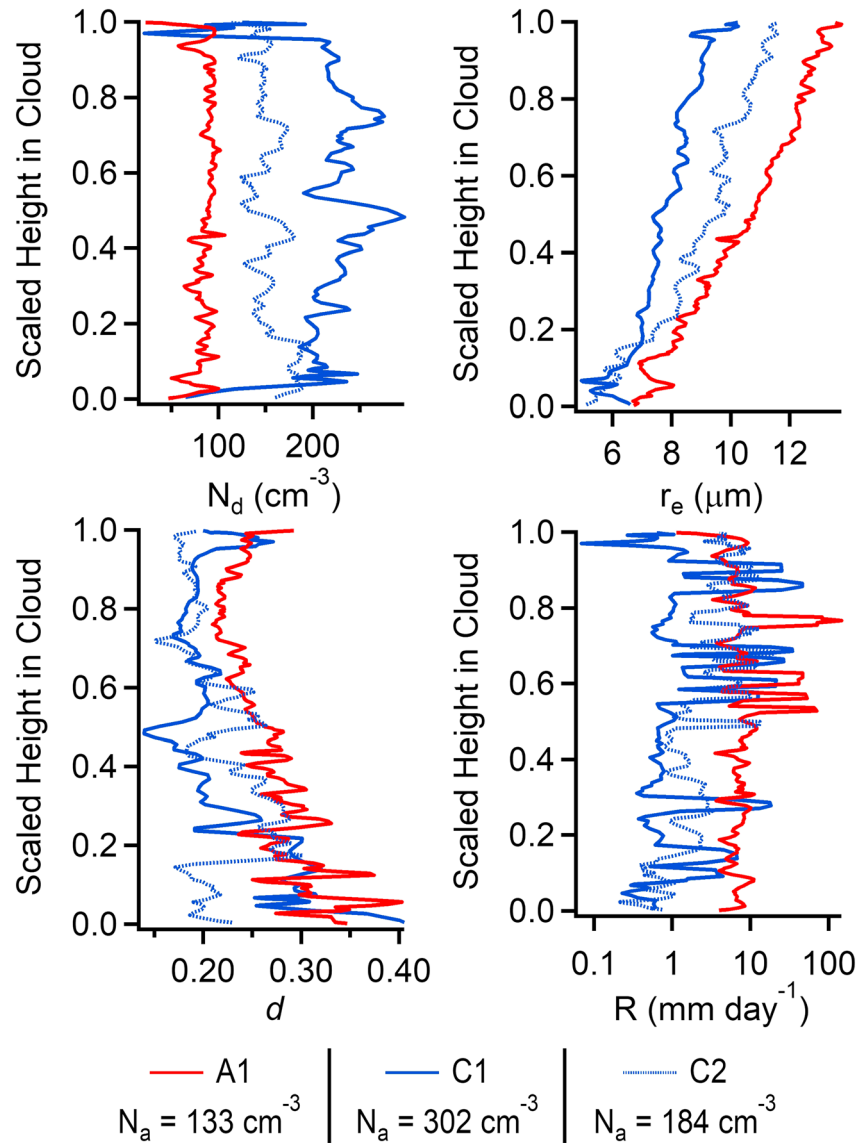
Figure 7. Vertical profiles of cloud droplet number concentration (N_d), cloud droplet effective radius (r_e), cloud droplet dispersion (d), and rain rate (R) for cloud events with measured liquid water path (LWP$_{measured}$) in the range of 104–114 g/m^2. Cloud events in the lowest-adiabaticity (α) category (category A) are shown in red, while cloud events in the highest-α category are shown in blue. The subcloud aerosol concentration (N_a) is given for each cloud event.

d (0.26) and R (8.25 mm/day) for event A1 still exceeded those for the two cloud events in category C ($d = 0.18$ [0.24] and $R = 2.06$ [5.59] mm/day for C1 [C2]). In contrast to the first case study, Figure 10 shows that all three cloud events in this LWP$_{measured}$ range had fairly consistent rain droplet concentrations up to approximately 200 µm. However, the higher R for A1 appears to be most likely driven by larger rain droplets found in the middle region of the cloud.

Previous studies have shown the importance of droplet sedimentation in limiting the impact of cloud-top entrainment through the removal of liquid water from the cloud top (Ackerman et al., 2009; Bretherton et al., 2007; Dearden et al., 2018; de Lozar & Mellado, 2017). Gravitational settling rates for droplets are a function of droplet size, with larger droplets settling more rapidly. For the first case study, N_d (r_e) is consistently lower (higher) for the low-α case (Figure 7). However, upon examining the full spectrum (Figure 8) the presence of larger droplets in the upper portion of the cloud is seen for profiles C1 and C2. Therefore, it is plausible that increased sedimentation due to the presence of large droplets at cloud top for the high-α cases
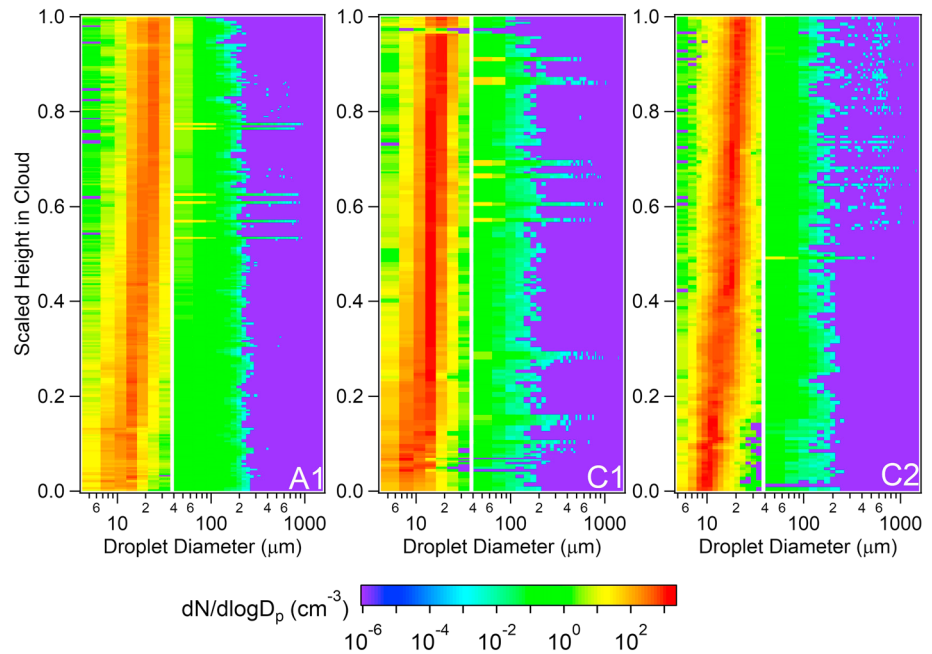
Figure 8. Cloud and rain droplet size distributions for one cloud event in the lowest-adiabaticity (α) category (A1) and two cloud events in the highest-α category (C1 and C2) with $LWP_{measured}$ between 104 and 114 g/m^2. The thin data gap around approximately 40 μm indicates the transition between cloud and rain droplet probes.

could contribute to reduced entrainment at cloud top. Interestingly, for the second case study, the low-α profile demonstrates a sharp reduction in N_d and r_e at cloud top (Figure 9), potentially signifying increased entrainment at cloud top. In this case, lower r_e and higher N_d at cloud top for the low-α profile, as compared to higher-α profiles, could indicate lower sedimentation rates, which is thought to increase cloud-top entrainment (Ackerman et al., 2009; Bretherton et al., 2007; Dearden et al., 2018; de Lozar & Mellado, 2017). This is also seen in the reduction of R at cloud top for A1, while C2 shows an increase in R at cloud top. The location of R in the cloud (i.e., cloud top or cloud base) can determine the subsequent impacts of R on LWP, with precipitation at cloud base leading to a decrease in LWP through water loss (Ackerman et al., 2004). Throughout the cloud depth, C1 shows the lowest average R and therefore may reside in the high-α category since LWC losses due to precipitation are minimized.

Variability in the relationships between the vertical profiles of these microphysical properties (N_a, N_d, r_e, d, and R) and α is seen in these two case studies. Further analysis is needed to determine conditions under which water loss mechanisms, such as entrainment and precipitation, are minimized or maximized. Additional measurements can also help learn about processes that may buffer the response in the cloud properties examined here to aerosol perturbations (Stevens & Feingold, 2009).

3.3. Cloud-Top Microphysical Properties

Characterization of microphysical properties at cloud top is important for validating assumptions made about cloud characteristics based on satellite retrievals of cloud-top properties. Entrainment mixing at cloud top can impact these retrievals (Brenguier et al., 2000). Cloud α has been used as a proxy for the characterization of entrainment mixing (Kim et al., 2008). In order to examine the changes, possibly due to cloud-top entrainment, in cloud-top properties as a function of α, parameters were compared between the top 20% (T_{20}) by height and bottom 80% (B_{80}) of each cloud event. Figure 11 shows the ratio of T_{20}:B_{80} for cloud microphysical properties N_d, r_e, and log(R). The difference in means between categories A and C was found to be statistically significant, based on a p value <0.05 using a two-tailed t test, for the T_{20}:B_{80} ratios for N_d (cloud droplet-only spectrum) and log(R). With increasing α, clouds demonstrate more homogeneity in N_d and r_e between the top and body of the cloud for the cloud droplet-only spectrum. However, for the full droplet spectrum, r_e shows a larger discrepancy between T_{20} and B_{80} with increasing α. This may be due to larger R in the top
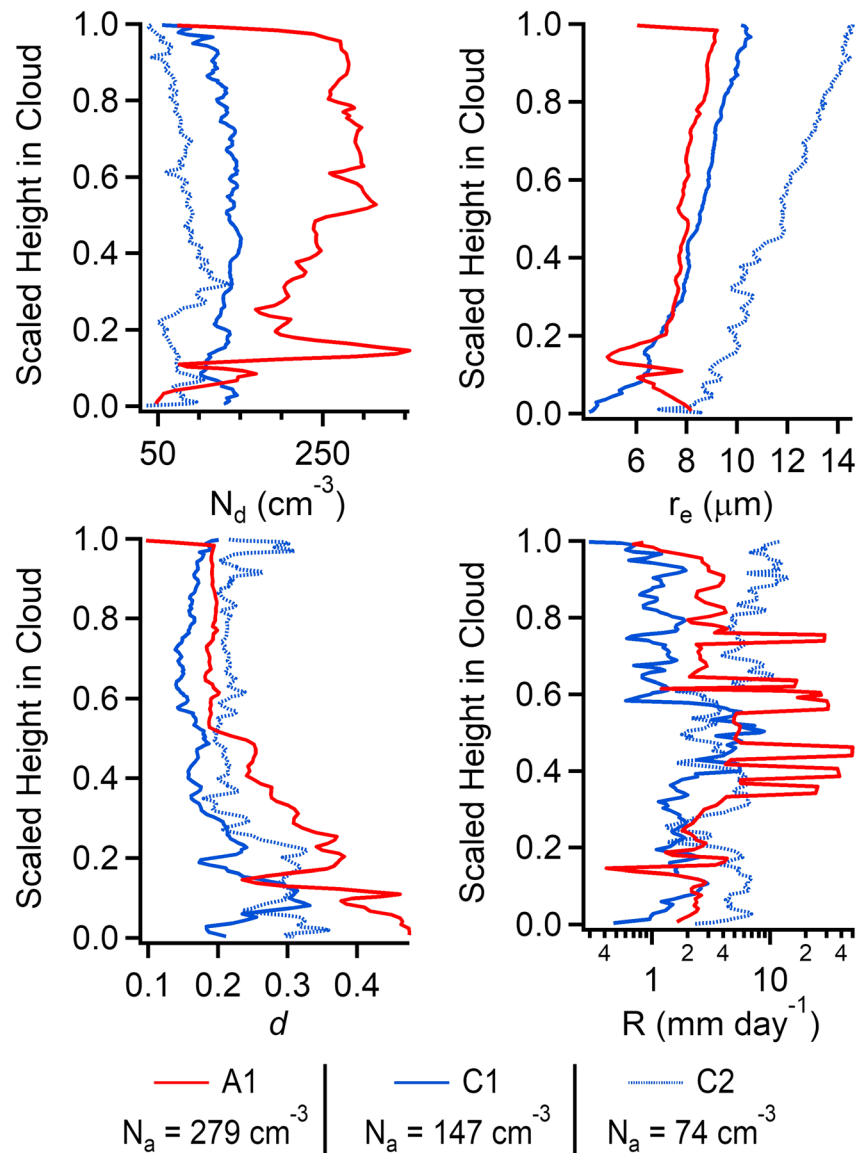
Figure 9. Same as Figure 7 except for cloud events with $LWP_{measured}$ = 131.5–141.5 g/m^2.

of the cloud as compared to the bottom in high-α cases (Figure 11c), which could correspond to more numerous larger droplets at the top of the cloud as compared to the bottom. Furthermore, the less-adiabatic clouds are characterized by less drizzle at the top of cloud as compared to the rest of the cloud. This result is in agreement with previous simulations that have linked increased cloud-top entrainment with decreased precipitation at cloud top (Ackerman et al., 2004). Those authors also note that the location of precipitation in a cloud can impact the effect of the precipitation on $LWP_{measured}$. Enhanced precipitation at cloud base (versus cloud top) in low-α clouds is also consistent with more effective scavenging of subcloud aerosol, as has been suggested already (e.g., Figures S1–S11).

Cloud-top microphysical properties can be impacted by entrainment of air from above cloud top and the amount of moisture contained in this above-cloud air. The average RH of air up to 30 m above cloud top was calculated using the measured temperature and dew point temperature above cloud (Buck, 1981). The range of 30 m was chosen due to previous work showing that the average entrainment interface layer depth in this study region is approximately 30 m (Dadashazar et al., 2018). Unsaturated air mixing at cloud top could lead to a decrease in LWC due to both inhomogeneous and homogeneous mixing. Evaporation
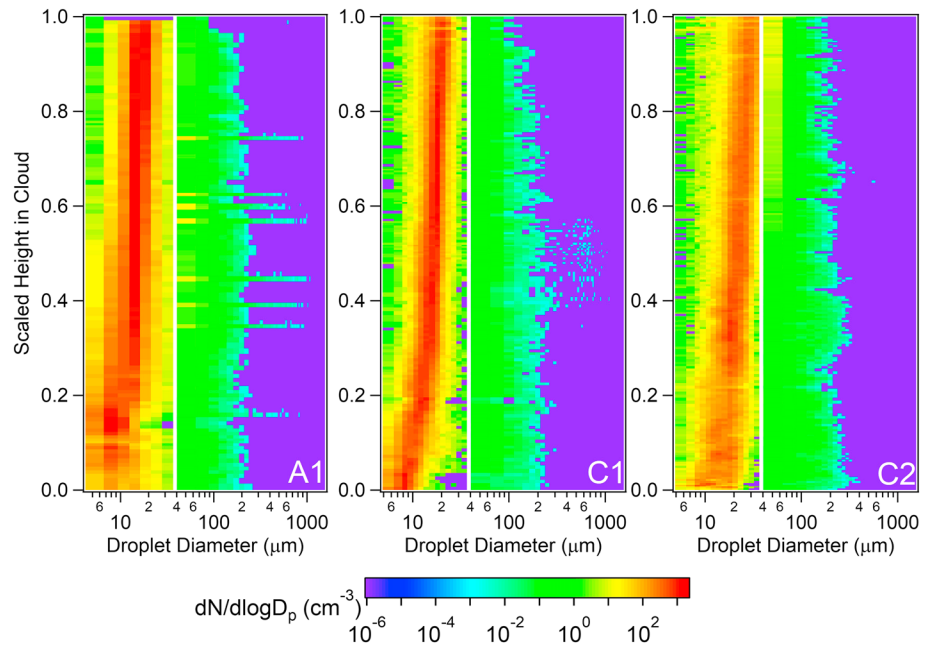
Figure 10. Same as Figure 8 except for cloud events with LWP$_{measured}$ = 131.5–141.5 g/m^2.

due to mixing with unsaturated air could lead to a decrease in r_e at cloud top. As shown in Figure S15 in supporting information, the ratio of r_e T$_{20}$:B$_{80}$ is reduced as RH decreases above cloud top, indicating that entrainment of drier air from above cloud may be more effective at causing evaporation from cloud droplets. In contrast, the ratio of N_d T$_{20}$:B$_{80}$ decreases with increasing RH above cloud. However, because
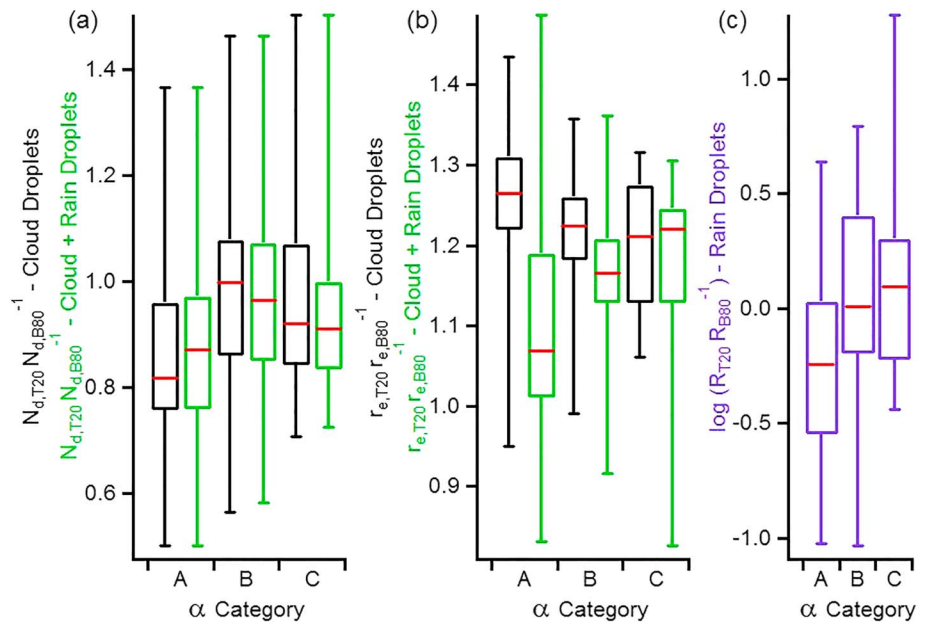

Figure 11. Box and whisker plots showing minimum and maximum values for the whiskers, 25th–75th percentile for the boxes, and median values as horizontal lines in each box. The 86 cloud events were divided into three α categories. The ratio between the top 20% (T$_{20}$) of the cloud (by height) and bottom 80% (B$_{80}$) of the cloud in each of the three α categories are shown for a droplet number concentration (N_d), (b) droplet effective radius (r_e), and (c) rain rate (R). For panels (a) and (b), the properties are shown for the cloud droplet-only spectrum (black) and the full (cloud and rain) droplet spectrum (green), while for panel (c), only the rain droplet spectrum (purple) is used for determination of R.

the amount of entrainment mixing was not quantified, it is difficult to determine the extent to which conditions above cloud, including RH, would impact microphysical properties in the cloud.

3.4. Comparison With MODIS Retrievals

Remote-sensing studies of cloud properties provide an alternative to the spatiotemporal restrictions associated with in situ airborne studies. In contrast to active remote sensing, where instrumentation produces and samples its own radiation, passive remote sensing measures emissions and reflections of naturally produced radiation. The MODIS uses passive remote sensing to observe radiation in numerous bands ranging from visible to infrared portions of the electromagnetic spectrum (Platnick et al., 2003). While different wavelengths may penetrate to various depths in the cloud, properties and structure in the upper portion of the cloud are most influential on remote-sensing retrievals (Platnick, 2000).

One important microphysical property of clouds, especially in regards to ACI studies, is N_d. However, N_d cannot be directly determined using current passive remote-sensing measurements but rather is calculated using a combination of other remotely sensed properties, such as r_e and cloud optical thickness (τ; Grosvenor et al., 2018). The retrievals of τ and r_e by MODIS utilize a combination of Sun-reflected visible and infrared spectral measurements (Nakajima & King, 1990). Previous studies have attempted to compare in situ N_d measurements with N_d calculated using retrieved properties from remote-sensing platforms, such as MODIS on NASA's Terra and Aqua satellites. In a study focused on the region over the Southeastern Pacific Ocean, Min et al. (2012) found that the inclusion of α in the calculation of N_d using remote-sensing retrievals provided better agreement with in situ data. Those authors noted that α differences in other global locations could drive changes in the formulation of N_d, motivating an analogous analysis for the NE Pacific.

Following the method of Min et al. (2012), 5-km-averaged MODIS retrievals were used only for cases with cloud fraction >0.95 and ≤1 hr between the time of the satellite overpass and in situ data collection. Of the 86 cloud events analyzed, 29 cases met these criteria, one of which was excluded from analysis due to very high values of in situ N_d. For the cloud events meeting the MODIS retrieval criteria, 23 of the 29 cloud events had whole cloud mean R in the light-drizzle range, three events had no R data available, and the remaining three events had cloud mean R in the medium-drizzle range ($0.3 < R < 0.5$ mm/hr, as defined in the American Meteorological Society's Glossary). Using retrievals of r_e and τ from MODIS, N_d was calculated using both equation (5) (Bennartz, 2007) and its modification, equation (6), with the inclusion of α (Min et al., 2012):

$$N_d = \frac{(\Gamma_{ad})^{\frac{1}{2}}}{k} \frac{10^{\frac{1}{2}}}{4\pi \rho_w^{\frac{1}{2}}} \frac{\tau^{\frac{1}{2}}}{r_e^{\frac{5}{2}}} \tag{5}$$

$$N_d = \alpha^{\frac{1}{2}} \frac{(\Gamma_{ad})^{\frac{1}{2}}}{k} \frac{10^{\frac{1}{2}}}{4\pi \rho_w^{\frac{1}{2}}} \frac{\tau^{\frac{1}{2}}}{r_e^{\frac{5}{2}}} \tag{6}$$

While equation (6) explicitly includes α, Bennartz (2007) did account for the subadiabatic structure of clouds worldwide by multiplying Γ_{ad} by 0.8 in equation (5). For this study, the average value of Γ_{ad} found for the study region was used ($\Gamma_{ad} = 2.332 \times 10^{-3}$ g/m^4). The parameter k, which is related to droplet spectral shape and equals 1 for a monodisperse droplet population, was calculated for the 86 cloud events as a function of skewness (s) and d (Lu & Seinfeld, 2006):

$$k = \frac{(1+d^2)^3}{(sd^3 + 1 + 3d^2)^2} \tag{7}$$

The average value for k in the top 20% of the cloud for the 86 cloud events was found to be 0.88 ± 0.04, similar to previous measurements of marine clouds ($k = 0.80 ± 0.07$ from Martin et al., 1994).

Figure 12 compares N_d as calculated using MODIS retrievals versus N_d from airborne data, determined as the average of N_d measured for the top 20% of the cloud by height. In Figure 12a, N_d is calculated using equation (5) without consideration of subadiabatic behavior. However, for Figures 12b and 12c, N_d was
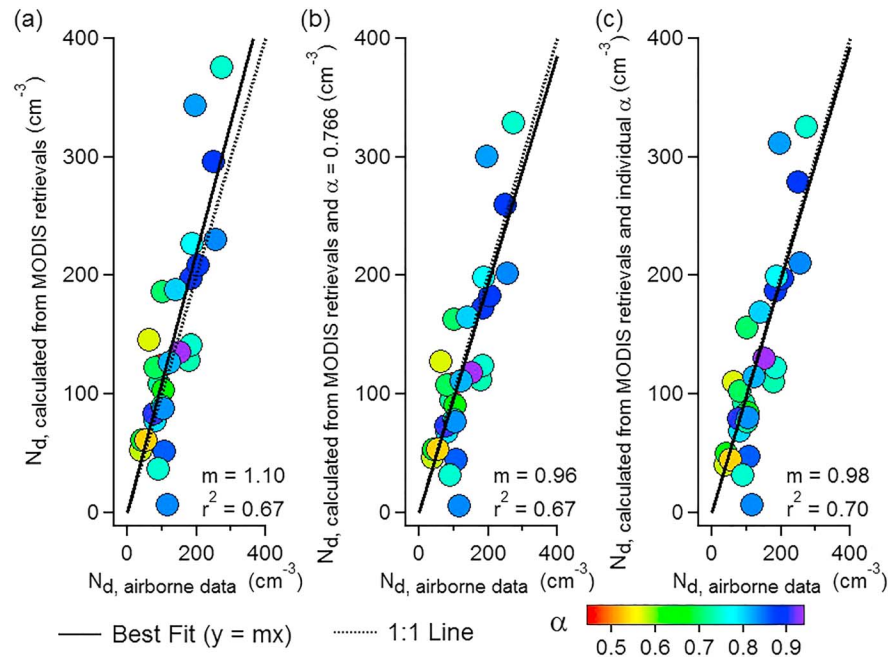
Figure 12. Comparison of cloud droplet number concentration (N_d), as calculated from 5-km MODIS retrievals, versus in situ airborne measurements in the top 20% of the cloud by height. Calculated N_d in panel (a) was determined using equation (5), while panels (b) and (c) include corrections for α (via equation (6)) using the average α for the study region and α from individual cases, respectively. The slope (m) of the linear best fit ($y = mx$) and a reference line of slope = 1 are shown for the three panels.

calculated using equation (6) and either the average α for the study region (Figure 12b) or α for each case (Figure 12c). Included in the supporting information is a residual plot quantifying the difference between the linear best fit values and individual events (Figure S16). For the case without considering α in the calculation of N_d, the slope is greater than 1, indicating that the N_d calculated from MODIS retrievals is an overprediction as compared to the in situ data. Accounting for α improves the predictions by driving the slope closer to unity, albeit less than 1, indicating an underprediction of N_d. The best agreement between the remote retrievals and airborne data was found when the individual α for the study region was used in equation (6).

4. Conclusions

This study has examined the adiabatic and microphysical structure of 86 cloud events over the NE Pacific Ocean using a combination of airborne data from four field campaigns and satellite remote-sensing retrievals. For the cloud events analyzed, the average α was found to be 0.766 ± 0.134, while H and α were observed to be negatively correlated. LWC was also observed to decrease with height in the upper portion of the cloud events, in contrast with adiabatic predictions.

In order to examine the dependence of vertical profiles of microphysical cloud properties on α, cloud events were binned by constant $LWP_{measured}$ to limit meteorological influences. In most cases, the less-adiabatic clouds exhibited lower N_d, higher r_e, higher d, higher R, and lower subcloud N_a. However, as shown in two case studies, these relationships did exhibit some differences, warranting future analysis. Variability in microphysical properties was also examined for each cloud thickness fifth for both the cloud droplet and full droplet (cloud and rain) spectra. The inclusion of the rain droplets, as compared to only cloud droplets, increased the d for the low-α cases by 17.8–26.6% on average for each cloud thickness fifth, as compared to only 9.6–12.4% on average for the high-α cases.

Because some satellite remote-sensing products focus on cloud top, the relationship between microphysical properties in the top 20% of the cloud versus the bottom 80% of the cloud were examined as a function of α.

When considering the cloud droplet-only spectrum, the higher-α clouds showed ratios of T_{20}:B_{80} closer to unity for N_d and r_e. However, this trend reversed when considering the full droplet spectrum r_e. Low-α cloud events showed on average a decrease in R for the T_{20}, while high-α cloud events had on average an increase in R at cloud top.

To understand the importance of α for remote-sensing retrievals, N_d was calculated using retrievals of r_e and τ from MODIS; considering α in the calculation resulted in better agreement with in situ data. Further analysis to evaluate additional impacts of α on remote-sensing retrievals, especially with regard to improving satellite-based N_d products, is warranted (e.g., Grosvenor et al., 2018). While the NE Pacific is an important region for marine stratocumulus clouds, additional analysis is needed for other regions around the world, including those that can allow α to be constrained across a greater range of environmental conditions (e.g., lower-troposphere stability conditions; see Wood & Bretherton, 2006) and cloud types (e.g., cumulus; see Lu et al., 2008). This would assist with improved assumptions in retrieval algorithms and models that aim to quantify cloud properties. Furthermore, development of remote-sensing technology and associated data processing algorithms (e.g., to quantify N_d) with reduced sensitivity to α would benefit future cloud studies (e.g., Painemal & Zuidema, 2011; Szczodrak et al., 2001).

References

Ackerman, A. S., Kirkpatrick, M. P., Stevens, D. E., & Toon, W. B. (2004). The impact of humidity above stratiform clouds on indirect aerosol climate forcing. *Nature*, *432*(7020), 1014–1017. https://doi.org/10.1038/nature03174

Ackerman, A. S., vanZanten, M. C., Stevens, B., Savic-Jovcic, V., Bretherton, C. S., Chlond, A., Golaz, J. C., et al. (2009). Large-Eddy simulations of a drizzling, stratocumulus-topped marine boundary layer. *Monthly Weather Review*, *137*(3), 1083–1110. https://doi.org/10.1175/2008mwr2582.1

Albrecht, B. A., Fairall, C. W., Tomson, D. W., White, A. B., Snider, J. B., & Schubert, W. H. (1990). Surface-based remote sensing of the observed and the adiabatic liquid water content of stratocumulus clouds. *Geophysical Research Letters*, *17*(1), 89–92. https://doi.org/10.1029/GL017i001p00089

Albrecht, B. A., Penc, R. S., & Schubert, W. H. (1985). An observational study of cloud-topped mixed layers. *Journal of the Atmospheric Sciences*, *42*(8), 800–822. https://doi.org/10.1175/1520-0469(1985)042<0800:aosoct>2.0.co;2

Baker, M. B., Blyth, A. M., Carruthers, D. J., Choularton, T. W., Fullarton, G., Gay, M. J., Latham, J., et al. (1982). Field studies of the effect of entrainment upon the structure of clouds at Great Dun Fell. *Quarterly Journal of the Royal Meteorological Society*, *108*(458), 899–916. https://doi.org/10.1002/qj.49710845810

Bennartz, R. (2007). Global assessment of marine boundary layer cloud droplet number concentration from satellite. *Journal of Geophysical Research*, *112*, D02201. https://doi.org/10.1029/2006JD00754

Boers, R., Jensen, J. B., Krummel, P. B., & Gerber, H. (1996). Microphysical and short-wave radiative structure of wintertime stratocumulus clouds over the Southern Ocean. *Quarterly Journal of the Royal Meteorological Society*, *122*(534), 1307–1339. https://doi.org/10.1002/qj.49712253405

Brenguier, J.-L. (1991). Parameterization of the condensation process: A theoretical approach. *Journal of the Atmospheric Sciences*, *48*(2), 264–282. https://doi.org/10.1175/1520-0469(1991)048<0264:POTCPA>2.0.CO;2

Brenguier, J.-L., Pawlowska, H., & Schüller, L. (2003). Cloud microphysical and radiative properties for parameterization and satellite monitoring of the indirect effect of aerosol on climate. *Journal of Geophysical Research*, *108*(D15), 8632. https://doi.org/10.1029/2002JD002682

Brenguier, J.-L., Pawlowska, H., Schüller, L., Preusker, R., Fischer, J., & Fouquart, Y. (2000). Radiative properties of boundary layer clouds: Droplet effective radius versus number concentration. *Journal of the Atmospheric Sciences*, *57*(6), 803–821. https://doi.org/10.1175/1520-0469(2000)057<0803:RPOBLC>2.0.CO;2

Bretherton, C. S., Blossey, P. N., & Uchida, J. (2007). Cloud droplet sedimentation, entrainment efficiency, and subtropical stratocumulus albedo. *Geophysical Research Letters*, *34*, L03813. https://doi.org/10.1029/2006GL027648

Buck, A. L. (1981). New equations for computing vapor pressure and enhancement factor. *Journal of Applied Meteorology*, *20*(12), 1527–1532. https://doi.org/10.1175/1520-0450(1981)020<1527:nefcvp>2.0.co;2

Burnet, F., & Brenguier, J.-L. (2007). Observational study of the entrainment-mixing process in warm convective clouds. *Journal of the Atmospheric Sciences*, *64*(6), 1995–2011. https://doi.org/10.1175/jas3928.1

Chen, Y. C., Christensen, M. W., Xue, L., Sorooshian, A., Stephens, G. L., Rasmussen, R. M., & Seinfeld, J. H. (2012). Occurrence of lower cloud albedo in ship tracks. *Atmospheric Chemistry and Physics*, *12*(17), 8223–8235. https://doi.org/10.5194/acp-12-8223-2012

Chin, H.-N. S., Rodriguez, D. J., Cederwall, R. T., Chuang, C. C., Grossman, A. S., Yio, J. J., Fu, Q., et al. (2000). A microphysical retrieval scheme for continental low-level stratiform clouds: Impacts of the subadiabatic character on microphysical properties and radiation budgets. *Monthly Weather Review*, *128*(7), 2511–2527. https://doi.org/10.1175/1520-0493(2000)128<2511:AMRSFC>2.0.CO;2

Dadashazar, H., Braun, R., Crosbie, E., Chuang, P., Woods, R., Jonsson, H., & Sorooshian, A. (2018). Aerosol characteristics in the entrainment interface layer in relation to the marine boundary layer and free troposphere. *Atmospheric Chemistry and Physics*, *18*(3), 1495–1506. https://doi.org/10.5194/acp-18-1495-2018

de Lozar, A., & Mellado, J. P. (2017). Reduction of the entrainment velocity by cloud droplet sedimentation in stratocumulus. *Journal of the Atmospheric Sciences*, *74*(3), 751–765. https://doi.org/10.1175/jas-d-16-0196.1

Dearden, C., Hill, A., Coe, H., & Choularton, T. (2018). The role of droplet sedimentation in the evolution of low-level clouds over southern West Africa. *Atmospheric Chemistry and Physics*, *18*(19), 14,253–14,269. https://doi.org/10.5194/acp-18-14253-2018

Duong, H. T., Sorooshian, A., & Feingold, G. (2011). Investigating potential biases in observed and modeled metrics of aerosol-cloud-precipitation interactions. *Atmospheric Chemistry and Physics*, *11*(9), 4027–4037. https://doi.org/10.5194/acp-11-4027-2011

Feingold, G., Remer, L. A., Ramaprasad, J., & Kaufman, Y. J. (2001). Analysis of smoke impact on clouds in Brazilian biomass burning regions: An extension of Twomey's approach. *Journal of Geophysical Research*, *106*(D19), 22,907–22,922. https://doi.org/10.1029/2001JD000732

Gerber, H., Arends, B. G., & Ackerman, A. S. (1994). New microphysics sensor for aircraft use. *Atmospheric Research*, *31*(4), 235–252. https://doi.org/10.1016/0169-8095(94)90001-9

Gerber, H., Frick, G., Malinowski, S. P., Jonsson, H., Khelif, D., & Krueger, S. K. (2013). Entrainment rates and microphysics in POST stratocumulus. *Journal of Geophysical Research: Atmospheres*, *118*, 12,094–12,109. https://doi.org/10.1002/jgrd.50878

Grosvenor, D. P., Sourdeval, O., Zuidema, P., Ackerman, A., Alexandrov, M. D., Bennartz, R., Boers, R., et al. (2018). Remote sensing of droplet number concentration in warm clouds: A review of the current state of knowledge and perspectives. *Reviews of Geophysics*, *56*, 409–453. https://doi.org/10.1029/2017RG000593

Janssen, R. H. H., Ganzeveld, L. N., Kabat, P., Kulmala, M., Nieminen, T., & Roebeling, R. A. (2011). Estimating seasonal variations in cloud droplet number concentration over the boreal forest from satellite observations. *Atmospheric Chemistry and Physics*, *11*(15), 7701–7713. https://doi.org/10.5194/acp-11-7701-2011

Kim, B.-G., Miller, M. A., Schwartz, S. E., Liu, Y., & Min, Q. (2008). The role of adiabaticity in the aerosol first indirect effect. *Journal of Geophysical Research*, *113*, D05210. https://doi.org/10.1029/2007JD008961

Kim, Y.-J., Kim, B.-G., Miller, M., Min, Q., & Song, C.-K. (2012). Enhanced aerosol-cloud relationships in more stable and adiabatic clouds. *Asia-Pacific Journal of Atmospheric Sciences*, *48*(3), 283–293. https://doi.org/10.1007/s13143-012-0028-0

Kubar, T. L., Hartmann, D. L., & Wood, R. (2009). Understanding the importance of microphysics and macrophysics for warm rain in marine low clouds. Part I: Satellite observations. *Journal of the Atmospheric Sciences*, *66*(10), 2953–2972. https://doi.org/10.1175/2009JAS3071.1

Lim, K.-S. S., Riihimaki, L., Comstock, J. M., Schmid, B., Sivaraman, C., Shi, Y., & McFarquhar, G. M. (2016). Evaluation of long-term surface-retrieved cloud droplet number concentration with in situ aircraft observations. *Journal of Geophysical Research: Atmospheres*, *121*, 2318–2331. https://doi.org/10.1002/2015JD024082

Liu, Y., & Daum, P. H. (2004). Parameterization of the autoconversion process. Part I: Analytical formulation of the Kessler-type parameterizations. *Journal of the Atmospheric Sciences*, *61*(13), 1539–1548. https://doi.org/10.1175/1520-0469(2004)061<1539:potapi>2.0.co;2

Liu, Y., Daum, P. H., Guo, H., & Peng, Y. (2008). Dispersion bias, dispersion effect, and the aerosol–cloud conundrum. *Environmental Research Letters*, *3*(4), 045021. https://doi.org/10.1088/1748-9326/3/4/045021

Lu, C., Liu, Y., & Niu, S. (2011). Examination of turbulent entrainment-mixing mechanisms using a combined approach. *Journal of Geophysical Research*, *116*, D20207. https://doi.org/10.1029/2011JD015944

Lu, M.-L., Feingold, G., Jonsson, H. H., Chuang, P. Y., Gates, H., Flagan, R. C., & Seinfeld, J. H. (2008). Aerosol-cloud relationships in continental shallow cumulus. *Journal of Geophysical Research*, *113*, D15201. https://doi.org/10.1029/2007JD009354

Lu, M.-L., & Seinfeld, J. H. (2006). Effect of aerosol number concentration on cloud droplet dispersion: A large-eddy simulation study and implications for aerosol indirect forcing. *Journal of Geophysical Research*, *111*, D02207. https://doi.org/10.1029/2005JD006419

MacDonald, A. B., Dadashazar, H., Chuang, P. Y., Crosbie, E., Wang, H. L., Wang, Z., Jonsson, H. H., et al. (2018). Characteristic vertical profiles of cloud water composition in marine stratocumulus clouds and relationships with precipitation. *Journal of Geophysical Research: Atmospheres*, *123*, 3704–3723. https://doi.org/10.1002/2017JD027900

Martin, G. M., Johnson, D. W., & Spice, A. (1994). The measurement and parameterization of effective radius of droplets in warm stratocumulus clouds. *Journal of the Atmospheric Sciences*, *51*(13), 1823–1842. https://doi.org/10.1175/1520-0469(1994)051<1823:tmapoe>2.0.co;2

McComiskey, A., Feingold, G., Frisch, A. S., Turner, D. D., Miller, M. A., Chiu, J. C., Min, Q., et al. (2009). An assessment of aerosol-cloud interactions in marine stratus clouds based on surface remote sensing. *Journal of Geophysical Research*, *114*, D09203. https://doi.org/10.1029/2008JD011006

Merk, D., Deneke, H., Pospichal, B., & Seifert, P. (2016). Investigation of the adiabatic assumption for estimating cloud micro- and macrophysical properties from satellite and ground observations. *Atmospheric Chemistry and Physics*, *16*(2), 933–952. https://doi.org/10.5194/acp-16-933-2016

Miller, M. A., Jensen, M. P., & Clothiaux, E. E. (1998). Diurnal cloud and thermodynamic variations in the stratocumulus transition regime: A case study using in situ and remote sensors. *Journal of the Atmospheric Sciences*, *55*(13), 2294–2310. https://doi.org/10.1175/1520-0469(1998)055<2294:DCATVI>2.0.CO;2

Min, Q., Joseph, E., Lin, Y., Min, L., Yin, B., Daum, P. H., Kleinman, L. I., et al. (2012). Comparison of MODIS cloud microphysical properties with in-situ measurements over the Southeast Pacific. *Atmospheric Chemistry and Physics*, *12*(23), 11,261–11,273. https://doi.org/10.5194/acp-12-11261-2012

Nakajima, T., & King, M. D. (1990). Determination of the optical thickness and effective particle radius of clouds from reflected solar radiation measurements. Part I: Theory. *Journal of the Atmospheric Sciences*, *47*(15), 1878–1893. https://doi.org/10.1175/1520-0469(1990)047<1878:dotota>2.0.co;2

Noh, Y. J., Seaman, C. J., Vonder Haar, T. H., & Liu, G. S. (2013). In situ aircraft measurements of the vertical distribution of liquid and ice water content in midlatitude mixed-phase clouds. *Journal of Applied Meteorology and Climatology*, *52*(1), 269–279. https://doi.org/10.1175/Jamc-D-11-0202.1

Painemal, D., & Zuidema, P. (2011). Assessment of MODIS cloud effective radius and optical thickness retrievals over the Southeast Pacific with VOCALS-REx in situ measurements. *Journal of Geophysical Research*, *116*, D24206. https://doi.org/10.1029/2011JD016155

Pawlowska, H., Grabowski, W. W., & Brenguier, J.-L. (2006). Observations of the width of cloud droplet spectra in stratocumulus. *Geophysical Research Letters*, *33*, L19810. https://doi.org/10.1029/2006GL026841

Perry, R. H., & Green, D. W. (2008). *Perry's chemical engineers' handbook*. New York: McGraw-Hill.

Platnick, S. (2000). Vertical photon transport in cloud remote sensing problems. *Journal of Geophysical Research*, *105*(D18), 22,919–22,935. https://doi.org/10.1029/2000JD900333

Platnick, S., King, M. D., Ackerman, S. A., Menzel, W. P., Baum, B. A., Riedi, J. C., & Frey, R. A. (2003). The MODIS cloud products: Algorithms and examples from Terra. *IEEE Transactions on Geoscience and Remote Sensing*, *41*(2), 459–473. https://doi.org/10.1109/tgrs.2002.808301

Prabhakar, G., Ervens, B., Wang, Z., Maudlin, L. C., Coggon, M. M., Jonsson, H. H., Seinfeld, J. H., et al. (2014). Sources of nitrate in stratocumulus cloud water: Airborne measurements during the 2011 E-PEACE and 2013 NiCE studies. *Atmospheric Environment*, *97*, 166–173. https://doi.org/10.1016/j.atmosenv.2014.08.019

Rotstayn, L. D., & Liu, Y. (2003). Sensitivity of the first indirect aerosol effect to an increase of cloud droplet spectral dispersion with droplet number concentration. *Journal of Climate*, *16*(21), 3476–3481. https://doi.org/10.1175/1520-0442(2003)016<3476:sotfia>2.0.co;2

Rotstayn, L. D., & Liu, Y. (2005). A smaller global estimate of the second indirect aerosol effect. *Geophysical Research Letters*, *32*, L05708. https://doi.org/10.1029/2004GL021922

Sorooshian, A., Feingold, G., Lebsock, M. D., Jiang, H. L., & Stephens, G. L. (2010). Deconstructing the precipitation susceptibility construct: Improving methodology for aerosol-cloud precipitation studies. *Journal of Geophysical Research*, *115*, D17201. https://doi.org/10.1029/2009JD013426

Sorooshian, A., MacDonald, A. B., Dadashazar, H., Bates, K. H., Coggon, M. M., Craven, J. S., Crosbie, E., et al. (2018). A multi-year data set on aerosol-cloud-precipitation- meteorology interactions for marine stratocumulus clouds. *Scientific Data*, *5*, 180026. https://doi.org/10.1038/sdata.2018.26

Stephens, G. L., & Haynes, J. M. (2007). Near global observations of the warm rain coalescence process. *Geophysical Research Letters*, *34*, L20805. https://doi.org/10.1029/2007GL030259

Stevens, B., & Feingold, G. (2009). Untangling aerosol effects on clouds and precipitation in a buffered system. *Nature*, *461*(7264), 607–613. https://doi.org/10.1038/nature08281

Szczodrak, M., Austin, P. H., & Krummel, P. B. (2001). Variability of optical depth and effective radius in marine stratocumulus clouds. *Journal of the Atmospheric Sciences*, *58*(19), 2912–2926. https://doi.org/10.1175/1520-0469(2001)058<2912:Voodae>2.0.Co;2

Twomey, S. (1974). Pollution and the planetary albedo. *Atmospheric Environment*, *8*(12), 1251–1256. https://doi.org/10.1016/0004-6981(74)90004-3

Twomey, S. (1977). The influence of pollution on the shortwave albedo of clouds. *Journal of the Atmospheric Sciences*, *34*(7), 1149–1152. https://doi.org/10.1175/1520-0469(1977)034<1149:TIOPOT>2.0.CO;2.

Wood, R. (2012). Stratocumulus clouds. *Monthly Weather Review*, *140*(8), 2373–2423. https://doi.org/10.1175/MWR-D-11-00121.1

Wood, R., & Bretherton, C. S. (2006). On the relationship between stratiform low cloud cover and lower-tropospheric stability. *Journal of Climate*, *19*(24), 6425–6432. https://doi.org/10.1175/jcli3988.1

Wood, R., Kubar, T. L., & Hartmann, D. L. (2009). Understanding the importance of microphysics and macrophysics for warm rain in marine low clouds. Part II: Heuristic models of rain formation. *Journal of the Atmospheric Sciences*, *66*(10), 2973–2990. https://doi.org/10.1175/2009JAS3072.1

Yeom, J. M., Yum, S. S., Liu, Y., & Lu, C. (2017). A study on the entrainment and mixing process in the continental stratocumulus clouds measured during the RACORO campaign. *Atmospheric Research*, *194*, 89–99. https://doi.org/10.1016/j.atmosres.2017.04.028

Yum, S. S., Wang, J., Liu, Y., Senum, G., Springston, S., McGraw, R., & Yeom, J. M. (2015). Cloud microphysical relationships and their implication on entrainment and mixing mechanism for the stratocumulus clouds measured during the VOCALS project. *Journal of Geophysical Research: Atmospheres*, *120*, 5047–5069. https://doi.org/10.1002/2014JD022802

Zhang, G., Vivekanandan, J., & Brandes, E. (2001). A method for estimating rain rate and drop size distribution from polarimetric radar measurements. *IEEE Transactions on Geoscience and Remote Sensing*, *39*(4), 830–841. https://doi.org/10.1109/36.917906

Zhao, G., Chu, R., Zhang, T., Li, J., Shen, J., & Wu, Z. (2011). Improving the rainfall rate estimation in the midstream of the Heihe River Basin using raindrop size distribution. *Hydrology and Earth System Sciences*, *15*(3), 943–951. https://doi.org/10.5194/hess-15-943-2011